Monthly Notices
of the
ROYAL ASTRONOMICAL SOCIETY

MNRAS **441,** 73–85 (2014) doi:10.1093/mnras/stu528

Star-forming galactic contrails as a source of metal enrichment and ionizing radiation at high redshift⋆

Michael Rauch,[1]† George D. Becker,[2] Martin G. Haehnelt[2] and Jean-Rene Gauthier[3]

[1]*Carnegie Observatories, 813 Santa Barbara Street, Pasadena, CA 91101, USA*
[2]*Institute of Astronomy and Kavli Institute for Cosmology, Cambridge University, Madingley Road, Cambridge CB3 0HA, UK*
[3]*California Institute of Technology, Pasadena, CA 91125, USA*

Accepted 2014 March 13. Received 2014 March 13; in original form 2013 May 24

ABSTRACT

A spectroscopically detected Lyman α emitting halo at redshift 3.216 in the GOODS-N field is found to reside at the convergence of several line-emitting filaments. Spatially extended emission apparently by He II 1640 Å and several metal transitions is seen within several arcseconds from the position of the central galaxy. The $V = 24.9$ galaxy mainly responsible for the continuum emission at the centre of the halo has broad-band colours and spectral features consistent with a $z = 3.216$ star-forming galaxy. *Hubble Space Telescope* images show that some of the filaments coincide, in projection, with several, mostly blue galaxies, with pronounced head–tail structures partly aligned with each other. These objects, for which we cannot rule that they are foreground, chance projections in front of the high-redshift halo, are seen over an area with a linear extent of at least 12 arcsec. The broad-band images of some galaxies suggest the presence of ram-pressure stripping, including possible evidence for recent star formation in the stripped contrails. Spatial gradients in the appearance of several galaxies may represent a stream of galaxies passing from a colder to a hotter intergalactic medium. The release of the enriched interstellar medium from galaxies and the occurrence of star formation and stellar feedback in the galactic contrails suggest a mechanism for the metal enrichment of the high-redshift intergalactic medium that does not require long-range galactic winds. If these galaxies are at the same redshift as the Lyα halo, their very blue colours may be a consequence of the stripping of gas. A stripped stellar population and star formation in galactic contrails suggest promising sites for the escape of ionizing radiation from high-redshift galaxies.

Key words: galaxies: evolution – galaxies: haloes – galaxies: interactions – intergalactic medium – diffuse radiation.

1 INTRODUCTION

Long-slit, spectroscopic blind surveys targeting the H I Lyα emission line have the potential to deliver detailed and otherwise unavailable insights into the gas dynamics and, in conjunction with deep, space-based imaging, the star–gas interactions in protogalactic haloes and the intergalactic medium (IGM). Several surveys of this kind (Rauch et al. 2008; Rauch et al. 2011, Paper I; Rauch et al. 2013a, Paper II; and Rauch et al. 2013b, Paper III) have discovered a distinct subpopulation of extended, asymmetric Lyα emitters at $z \sim 3$, with a comoving space density of the order of 10^{-3} Mpc^{-3} and typical observed line fluxes of a few times 10^{-17} erg cm^{-2} s^{-1}. With a large number of processes capable of producing Lyα radiation, one may expect the emitters to be drawn from a highly inhomogeneous group of objects. However, the selection by Lyα emission is likely to favour galaxies in certain phases of their formation, when the stellar populations present and the gas dynamics are particularly conducive to the production and escape of Lyα photons. The peculiar spatial distribution and clustering behaviour of Lyα emitters suggests that environmental effects and interactions may play an important role in determining whether a galaxy appears as a Lyα emitter (e.g. Hamana et al. 2004; Hayashino et al. 2004; Kovac et al. 2007; Ouchi et al. 2009; Cooke et al. 2010; Zheng et al. 2011; Matsuda et al. 2012; Cooke, Omori & Ryan-Weber 2013). Indeed, all four extended emitters described so far in the papers in this series exhibit signs of interactions.

The duration of the processes leading to the production of ionizing radiation (e.g. the lifetimes of massive stars, AGN activity), as well as the astrophysical time-scales relevant for the emission of

⋆The data presented herein were obtained at the W.M. Keck Observatory, which is operated as a scientific partnership among the California Institute of Technology, the University of California and the National Aeronautics and Space Administration. The Observatory was made possible by the generous financial support of the W.M. Keck Foundation.

† E-mail: mr@obs.carnegiescience.edu

Lyα in high-redshift gaseous haloes (recombination- and resonance-line radiative-transfer time-scales) tend to be short compared to the dynamical time-scales and lifetimes of the general stellar population. Thus, the spectroscopic detection of such a halo amounts to a 'snapshot' of a particularly interactive phase in their formation, illuminated by a 'flash' of Lyα emission.

Among those extended Lyα emitters published to date, the first one showed diffuse stellar features, in addition to a clear detection of the infall of cold gas into an ordinary high-redshift galaxy (Paper I). Paper II described what may be a Milky way-sized halo with multiple galaxies hosting disturbed, partly young stellar populations. A thin filament apparently dominated by high equivalent width Lyα emission may reflect recent intrahalo star formation in a tidal tail or in the wake of a satellite galaxy. The third object, revealing the only case in this sample clearly related to non-stellar processes, is an AGN illuminating a satellite galaxy, possibly triggering the formation of very young stars in its halo (Paper III). The object examined in this paper is a large halo surrounded by emission line filaments, coinciding in projection with a group of distorted, mostly blue galaxies. As we shall argue below, the interaction in this case may be between the galaxies and a gaseous medium through which they move, stripping off part of the galactic gas and inducing star formation in their wake.

The observations are described in the next section, followed by a description of the galaxies coinciding with the gaseous halo. The presence of spatially extended metal emission, the nature of the filaments, and the energetics of the emission are then discussed. The paper concludes with a discussion of the likely nature of the phenomenon and its significance for the metal enrichment of the IGM and for the escape of photons responsible for its ionization.

2 OBSERVATIONS

The observations consist of a long-slit, spectroscopic blind survey, with the slit positioned in precise N–S orientation on the object J123647.05+621237.2 in the *Hubble Deep Field* North (HDFN). Data were taken with the LRIS (Oke et al. 1995; McCarthy et al. 1998; Steidel et al. 2004) B and R arms and the D560 dichroic, using the 600/4000 grism in 2×2 binning (blue side) and the 600/7500 grating in 1×1 binning (red side), through a custom long slit built from two slit segments with a combined size of 2 arcsec × 430 arcsec. The wavelength covered ranged from 3310 to 5794 Å for the blue arm and from 5538 to 8134 Å for the red arm. The slit-limited spectral resolution measured from a comparison lamp near the central wavelength in the blue for the 2 arcsec wide slit was approximately 7.7 Å full width at half-maximum (FWHM), corresponding to a velocity resolution of 517 km s^{-1}. Total exposure times of 35.8 h in the blue and 35 h in the red arm of LRIS were obtained in 2008 March, May, and 2009 April. The resulting 1σ surface brightness detection limit, measured for a 1 − □arcsec wide aperture, is approximately 1.1 × 10^{-19} erg cm^{-2} s^{-1}□″.

2.1 Identity of the emission line

The spectrum shows a strong emission complex with flux peaking near 5123.0 Å (vacuum; Fig. 1). An identification as H I Lyα at z = 3.21 is suggested by the large spatial extent of the line emission beyond the continuum, by the blue–red asymmetry typical of high-redshift Lyα emission lines, and by the drop in the continuum bluewards of the emission line, presumably caused by the Lyα forest (Fig. 2). Inspection of archival GOODS-N v2.0 images (Giavalisco et al. 2004; Fig. 5, top-right panel) shows the continuum source closest to the inferred slit position to be GOODS J123646.84+621608.1 (Giavalisco et al. 2004). This galaxy, which will be referred to from here on as object '1' (see Table 1 and the figures below), has additional ground-based broad imaging obtained by the Hawaii HDFN survey (Capak et al. 2004). Its colours ($U - B = 2.4$, $B - V = 0.7$, and $B - R = 0.9$, in their filter system) are compatible with those of a $z \sim 3$ high-redshift galaxy. Two published photometric redshift determinations give redshifts of 3.09 (Xue et al. 2011) and 0.378 (Conselice et al. 2011). The highly discrepant photometric redshifts presumably reflect the resemblance between the spectral regions encompassing a high-redshift Lyα line plus Lyα forest decrement and the wavelength region near a low-redshift [O II] 3728 doublet. The similarity is quite close, and with the low resolution, low signal-to-noise ratio data, neither alternative can be immediately dismissed. An unidentified absorption line at 5422 Å, together with part of the broad absorption line at 5477 Å could possibly be identified with absorption by Ca II H&K at $z = 0.378$ (as suggested to us by the referee). This redshift is exhibited by several galaxies within 2 arcmin of the present position. A redshift $z = 0.378$ would put the [O II] 3728 doublet surprisingly close to the observed wavelength position of the 5123 Å emission line, and even put the [O III] 5008 Å close to the wavelength of a $z = 3.21$ He II 1640 Å emission line. However, the velocity difference between Ca II H&K and [O II] 3728 would be of the order of 700 km s^{-1}, which would be hard to explain through

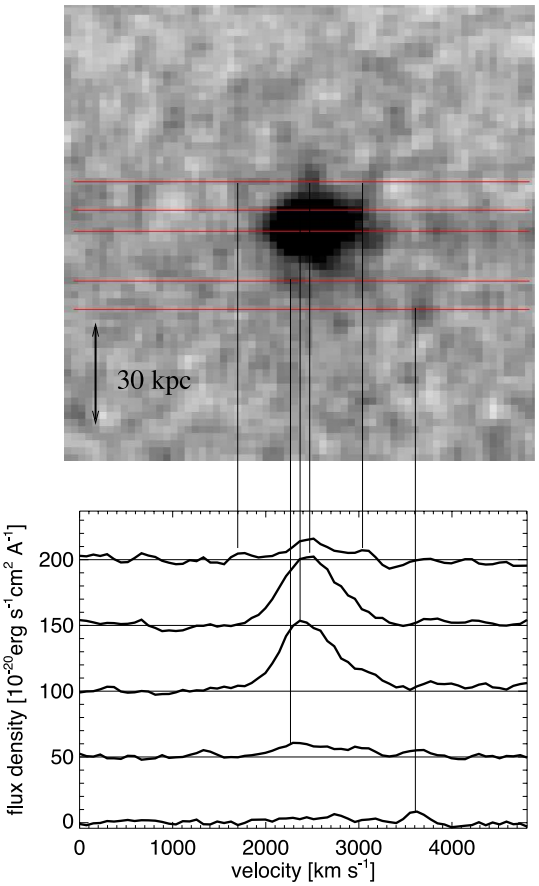

Figure 1. Two-dimensional, continuum-normalized spectrum of the 5123 Å emission line (top panel). The spatial extent along the slit (vertical direction) is 17.3 arcsec. The bottom panel shows one-dimensional spectra along the five cuts delineated in the top panel, extracted over three spatial pixels (0.81 arcsec).

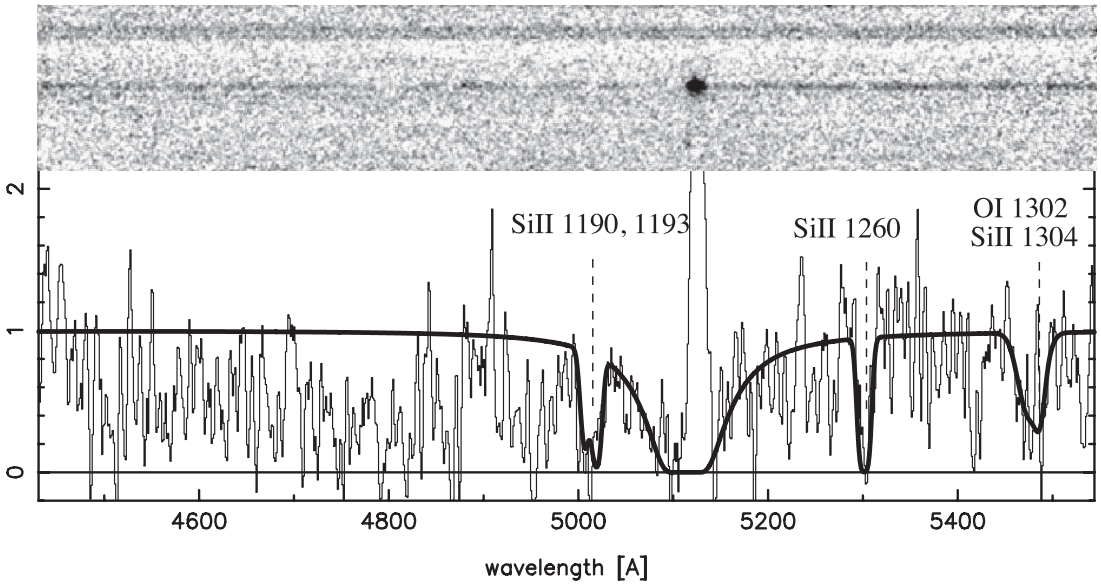

Figure 2. Two-dimensional LRIS-B spectrum (top) and one-dimensional, optimally extracted spectrum (bottom; thin solid line) with a single-component, simultaneous fit to H I, Si II, and O I at $z = 3.206\,07$ overlaid (solid line).

Table 1. Properties of the sources.

ID	GOODS-N[a]	V^a	$B - V^a$	V (Head)	$B - V$ (Head)	V (Tail)	$B - V$ (Tail)	B-band SFB (Tail) (mag/ □arcsec)
1	J123646.84+621608.1	24.90 ± 0.03	1.10 ± 0.11	25.60 ± 0.06	1.27 ± 0.10	27.07 ± 0.09	0.79 ± 0.19	26.32
2	J123646.42+621606.8	26.08 ± 0.09	0.10 ± 0.15	26.43 ± 0.07	0.42 ± 0.11	27.04 ± 0.09	0.16 ± 0.16	26.41
3	J123645.87+621604.0	26.27 ± 0.09	0.88 ± 0.27	26.45 ± 0.10	0.56 ± 0.25	27.14 ± 0.24	-0.37 ± 0.32	28.12
4	J123646.08+621603.9	26.82 ± 0.10	0.12 ± 0.18	27.20 ± 0.15	-0.14 ± 0.20	28.20 ± 0.20	$>2.80^b$	–
5	J123645.99+621601.6	27.54 ± 0.14	0.09 ± 0.24	28.18 ± 0.15	0.07 ± 0.21	27.89 ± 0.13	-0.01 ± 0.19	25.75
6	Not det.	–	–	27.64 ± 0.13	-0.01 ± 0.17	Point source	–	27.82
7	Not det.	–	–	–	–	31.12 ± 2.68	-3.53 ± 2.68	26.22
8	Not det.	–	–	27.15 ± 0.11	0.53 ± 0.16	> 29.01	$< -0.69^c$	28.04
9	Not det.	–	–	28.95 ± 0.90	-0.89 ± 1.00	Point source	–	28.57
10	J123647.09+621605.9	27.81 ± 0.18	-0.08 ± 0.27	27.92 ± 0.18	-0.39 ± 0.24	Point source	–	–

Comments: [a]Giavalisco et al. (2004); [b]adopting 1σ flux error for B; [c]adopting 1σ flux error for V.

an astrophysical scenario or as velocity shift induced by positional uncertainties across the (2 arcsec wide) slit. The possibility remains that the two absorption lines are indeed partly due to Ca II absorption by foreground gas at $z = 0.378$, coincident with the gaseous haloes of intervening galaxies. Other nearby galaxies within 16 arcsec from object 1 and with spectroscopic redshifts in the literature include objects at $z = 0.50$, 1.45, 2.44, and 0.85. Of possible interest for the redshift identification of the 5123 Å emission line is the presence of two close, faint, blue galaxies with similar morphology as object 1 (called objects '2' and '4' below) and photometric redshifts $z = 0.825$ and 0.900 (Conselice et al. 2011). A redshift of $z = 0.832$ could explain the strong emission line as blended Mg II 2796, 2804 Å emission. Experimentation shows that a line profile shape as observed, while not resembling the simple shape of the Mg II doublet, can be contrived from a superposition of multiple Mg II absorption and emission components. However, it requires multiple components separated in velocity space by over 1300 km s^{-1}, which may be unphysical. At least two of the filaments (the one denoted by $\gamma - \delta$ and the one ending in ϵ, in Fig. 5) sticking out at the bottom end of the halo have wavelength separations roughly consistent with the Mg II doublet and may be more plausibly caused by Mg II emission (at $z = 0.832$), even though the main halo may be caused by higher redshift ($z = 3.21$) Lyα emission.

While we are not able to rule out foreground contributions in either emission or absorption to the spectrum from intervening galaxies, on balance, most of the observed spectral features appear compatible with the interpretation of the line as $z = 3.21$ high-redshift Lyα emission. The emission region appears to reside in a flux depression that can be modelled as a damped Lyα absorption trough at $z = 3.206\,07 \pm 0.000\,60$, with H I column density $\log N_{\rm H\,I} = 21.376 \pm 0.065$. This redshift predicts well the positions of absorption lines Si II 1190, 1193, 1260, 1304, and O I 1302 (Fig. 2). Si II 1526 absorption (and possibly Si II* 1533 emission) may be present, too, in the red part of the spectrum, but, like Si IV 1393, 1402 and C IV 1548, 1550, is affected by the low signal-to-noise ratio and sky residuals. At the blue end, the continuum flux drops from $(6.05 \pm 0.67) \times 10^{-21}$ erg s^{-1}cm^{-2} Å^{-1} in the region between Lyβ and the Lyman limit to $(1.20 \pm 2.03) \times 10^{-21}$ erg s^{-1}cm^{-2} Å^{-1} bluewards of the Lyman limit, consistent with an optically thick Lyman limit absorption edge expected for such a large column density. Fig. 3 shows the blue end of the spectrum down to the putative Lyman limit. Even with the low signal-to-noise ratio and absorption by the Lyα forest, the blue end of our spectrum shows considerable similarities with the spectrum of a starburst galaxy redshifted to $z = 3.21$, here a FUSE spectrum of NGC1705 (Pellerin & Robert 2007), shown for comparison (dotted line).

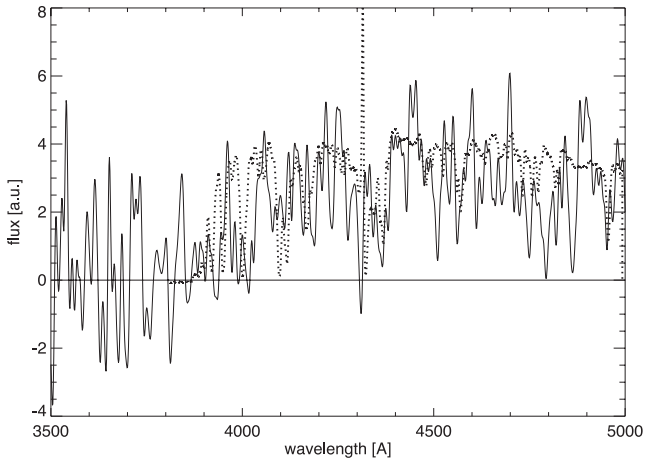

Figure 3. Section of the unnormalized 1D spectrum (solid line), smoothed with a 5-pixel boxcar filter, showing the spectrum above and below the Lyman limit (near an observed wavelength of 3840 Å), overplotted by a spectrum of the starburst galaxy NGC1705 (Pellerin & Robert 2007), redshifted to $z = 3.21$ (dotted line). The starburst template was scaled to match 1.25 times the flux of the object, crudely accounting for the average intergalactic absorption which is not present in the low-redshift template.

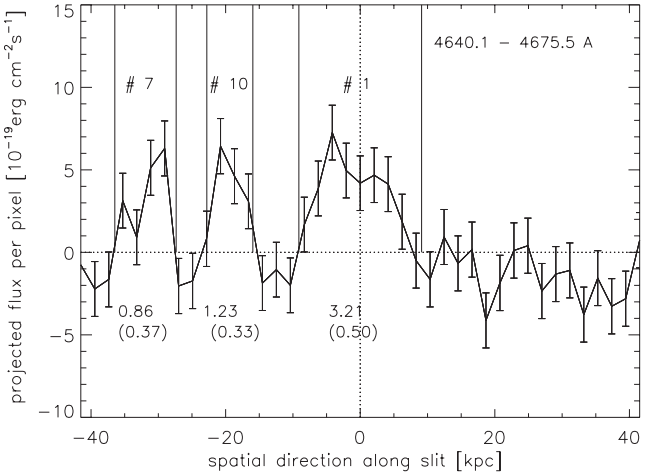

Figure 4. A spatial cut in the direction along the slit, between rest-frame wavelengths 4640.1–4675.5 Å, where the continua of the main galaxy 1 and the two fainter objects 7 and 10 can be observed most clearly. The numbers below the three windows marked as #7, #10, and #1 are the projected summed fluxes and 1σ errors in units of 10^{-18} erg cm^{-2} s^{-1} in the above wavelength range, and within the spatial windows indicated by vertical lines.

Accepting the identification as H I Lyα, the peak of the emission line corresponds to a redshift 3.2156 when fitted as a single Gaussian component. It exhibits an FWHM ∼910 km s^{-1}, and occurs 680 km s^{-1} redwards of the centre of the absorption trough. When fitted more appropriately with two Gaussian components, we find redshifts of 3.2173 ± 0.0010 and $3.214\,280 \pm 0.000\,46$, with widths (FWHM) of 850 and 380 km s^{-1} and a shift of 541 km s^{-1} between the absorption trough and the bluer of the two emission components.

The width of the Lyα line and its red shoulder may partly arise from the superposition of multiple sources (see below). After subtraction of the continuum trace, the total Lyα flux that passed through the slit is $(2.26 \pm 0.13) \times 10^{-17}$ erg cm^{-2} s^{-1}.

The emission line halo is remarkable in that several filaments extrude to distances of at least 27 proper kpc (in projection) away from the continuum position. At least three of these structures spatially overlap in projection with multiple features detected in the *Hubble Space Telescope* ACS *F435W* ('*B* band') image (RHS panels of Fig. 5). In an area extending to about 5 arcsec on either side of the slit, two highly distorted, tadpole-shaped galaxies (1 and 2; with object 1 producing the continuum in the spectrum) can be seen, Both have substructure with multiple cores of blue light in their heads (Figs 6 and 11). Several more extended low surface brightness features can be seen further afield (objects 3–7) partly also with (less distinctive) head and tail structures. Among these are blue sources with (objects 5 and 8) and without (object 10) tails, and at least one object (number 3) with an apparent linear size of more than 40 kpc (if at $z = 3.21$). None of these objects have independent redshift determinations, so any one of them could be a lower redshift, foreground source.

Circumstantial evidence, suggests, however, that some of them may be physically linked to the spectroscopically observed emission features. Of the features in the emission line halo, the central emission peak 'α' lines up, in projection, with tadpole 1 in the image, 'ζ' with the smudge near number 9, 'δ' with 7, and 'γ' with 10. The latter two also have very faint continua recognizable in some regions of the spectrum (e.g. between ∼4600 and 4800 Å; see Figs 2 and 4, and the top panel in Fig. 9) that spatially line up with the minor emission peaks, showing the $\gamma - \delta$ filament to be subtended by at least two galaxies. The other significant emission smudges with Greek letters, β and ϵ, plus the vaguely visible elongated features on either side of β may also have counterparts in the broad-band, with ϵ possibly related to object 4 (see below). The various white contours in the bottom-right panel of Fig. 5, are marking extraction windows used to determine the fluxes listed in Table 1. Even though the low surface brightness features are statistically significant detections (objects 3, 8, and 7 are 5.0, 4.4, and 8.1 σ excursions in the *B* band), some of them could be observational artefacts. The apparent association of the objects 1, 7, 10, and possibly 4 with emission line features at the same wavelength, and the simultaneous presence of several highly distorted objects and/or objects with similar (blue; $B - V \leq 0.12$)) colours suggest, however, that most of the features are real and part of the same physical environment. A search for objects with $B - V \leq 0.12$ in the field suggests that the group of the six bluest objects in the central 10 arcsec × 10 arcsec area represents a relative overdensity of a factor of 4.7 compared to the background density of such objects averaged over a 2 arcmin × 2 arcmin field, with a 1.4 per cent (3.6σ if Poissonian) probability of occurring by chance. This suggests a common origin of these objects, but it does not prove that they are at the same redshift as the Lyα emission, as these colours are very blue for $z \sim 3.21$, and may be more compatible with lower redshift, foreground galaxies, where the reddening by the intervening Lyα forest would be less prominent. Physical explanations for these colours will be discussed further below.

Further distorted objects in the *B* band occur to the N-W of the present region (not shown). If some of these belong to the same large-scale structure, the total maximum extent could be as large as 210 kpc proper. With the field being located near the edge of the GOODS-N imaging coverage, we cannot follow the structure further to the north.

3 GALAXY PROPERTIES

The various objects shown in the broad-band figure are listed with their identifying numbers in column 1 of Table 1, together with their name in the GOODS-N catalogue (where detected) in column 2.

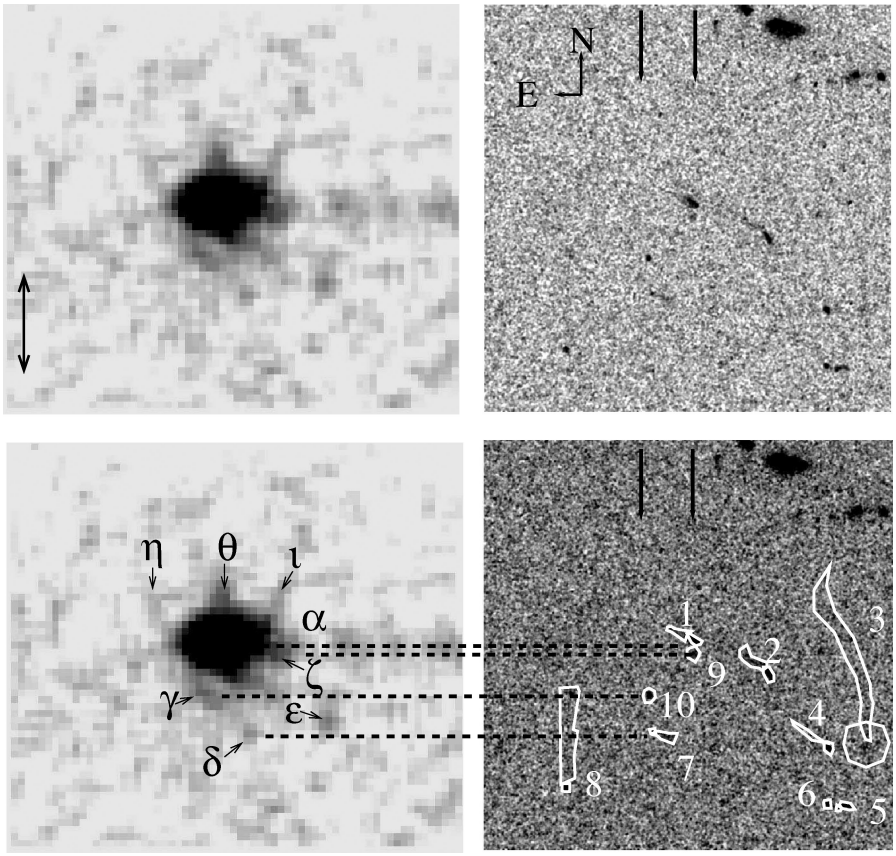

Figure 5. Two-dimensional Keck LRIS spectrum of the Lyα emission line region (left-hand panel) and ACS *B*-band (*F*435*W*) image (right-hand panel; smoothed with a 3×3 pixels boxcar filter). In the spectrum, the dispersion runs from left (blue) to right (red), and the N–S direction from top to bottom, with a spatial extent of 16 arcsec. For clarity, the bottom row of panels repeats the top row, but with annotations. The numbered white closed lines are the extraction windows used to obtain the flux measurements given in Table 1. The numbers refer to galaxies with broad-band detections listed in Table 1, the Greek letters to features in the 2D spectrum. The two black vertical lines at the top of the images indicate the approximate position of the slit, which was determined from a scheme minimizing the variance between the image collapsed perpendicular to the slit position and the spectrum. The spectrum on the left is shown over a velocity stretch of 4880 km s^{-1} and shows apparent filaments extending south from the continuum position out to at least 27 kpc proper (from the centre of the emitter to position δ) in projection along the slit, and further, faint protuberances appear to be sticking out to the north. The broad-band smudges seen in the image extend over at least about 90 kpc in the N–S direction and E–W directions. Several of the emission patches in the spectrum have counterparts in the *B*-band image (black dashed lines).

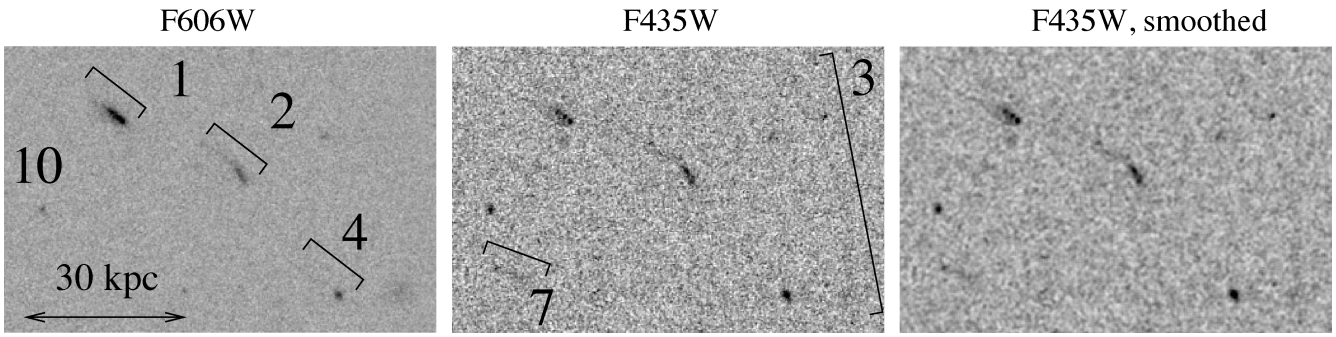

Figure 6. Broad-band images of several distressed galaxies to the S-W of the position of the Lyα halo. The size of each image is 10.2 arcsec × 6.7 arcsec, with N up and E to the left. The image is centred at 12:36:46.48 +62:16:06.16 (2000). The panels from left to right are: the ACS *F*606*W* (*V* band) image, the *F*435*W* (*B* band) image, and a version of the latter smoothed with a 3×3 boxcar filter. Object 1, less than an arcsec to the W from the centre of the slit, is the source of most of the continuum emission and possibly most of the Lyα in the spectrum. Brackets show the multiple apparent head and tail structures for several objects. For objects 1–4, the head appears to the S-W of the tail. Object 10 is a point source, whereas 7 has a less distinct shape, with a more E–W orientation and the peak flux occurring to the E. Note the multiple bright cores in the two tadpoles 1 and 2, seen in the rightmost panel. The *V*-band flux of object 4, if at $z = 3.21$, may be dominated by Lyα emission.

The GOODS-N broad-band B and $B - V$ colours (columns 3 and 4) are followed in columns 5–8 by the same quantities determined directly in extraction windows placed on the head and tail regions of the various objects shown in Fig. 5. Note that no corrections for extinction or intergalactic absorption have been applied. From the work by Meiksin (2006), we expect that a colour correction of about $\delta(B - V) \sim -0.4$ (for young star-forming galaxies at $z = 3.2$) needs to be added to the magnitudes in the table.

The magnitudes of the 'heads' show good correlation with the GOODS-N 'magbest' magnitudes where available for the same object. Because of the irregular apertures used, the absolute magnitudes are not precisely comparable among objects. The useful information mainly lies in the $B - V$ colours and their gradients between heads and tails. Objects 2, 4, 5, 6, 7, 9, and 10 are generally blue (overall $B - V < 0.12$ in the GOODS-N catalogue, or, where uncatalogued, in our apertures). We caution not to read too much into the formally very blue colours as the sometimes very large formal errors speak for themselves. However, there is a clear trend in that all the cases where there is a distinct head–tail shape (objects 1, 2, 3, 5, and 8), with the exception of object 4, have bluer tails than heads. The tendency for the tails to be bluer than the heads is different from the prevailing pattern for tadpole galaxies (e.g. Elmegreen & Elmegreen 2010), although in our case, strong Lyα emission from the heads (with its observed wavelength at $z = 3.2$ in the V band) could make them appear redder even though their continuum may be quite blue.

The Hawaii HDFN survey (Capak et al. 2004) has U-band and other broad-band detections for two of the objects (with about 75 per cent of the filter width probing a wavelength region below the $z = 3.21$ Lyman limit). As mentioned above, the colours of object 1 are clearly compatible with a $z \sim 3$ high-redshift galaxy. Object 2, however, has $U - B = 0.26$, $B - V = 0.08$, i.e. it is not even a partial U-band dropout. Object 10, while too faint to be included in the Capak et al. catalogue, shows faint flux below the Lyman limit in our spectrum. This could be an indication of these objects being at significantly lower redshift than 3.2. However, it is not clear whether the blue colours are necessarily incompatible with a high-redshift galaxy. Based on the observed rate of incidence of Lyman limit absorbers in the IGM (e.g. Prochaska, Worseck & O'Meara 2009), the probability of not having an intervening Lyman limit absorber in the line of sight to a $z = 3.21$ galaxy in the wavelength range of this particular U-band filter should be roughly between 0.3 and 0.6, i.e. considerable. In that case, the $\delta(U - B)$ due to intergalactic absorption could be small (e.g. Meiksin 2006), and the observed $U - B$ colour would reflect mainly the intrinsic continuum shape. The observed colours would still require weak or absent intrinsic Lyman limits and very blue intrinsic continuum slopes. A shallow Lyman limit discontinuity may be associated with an AGN, or with a population of young, metal-poor, hot stars (e.g. Schaerer 2003); UV radiation below the Lyman limit break may be boosted by the redistribution of stellar ionizing continuum (Inoue 2010). Very blue colours for galaxies could be a consequence of suppressed nebular emission and intrinsic absorption (Raiter, Schaerer & Fosbury 2010). These conditions may be associated with ram-pressure stripping, which would explain the extended morphologies as well, a possibility which we shall discuss below.

The object 4 is an interesting case in that the tail is only visible in the V band (Fig. 7), with a total flux of $(5.8 \pm 1.2) \times 10^{-17}$ erg cm^{-2} s^{-1}, corresponding to a 4.8σ detection. The situation here may be similar to the one presented in Paper II, a narrow filament of emission visible in only one broad-band, that may be glowing in Lyα, except that in the current situation, the Lyα line, due to its higher redshift, would be situated in the V band and not in B. Because of the low flux, other broad-band images do not provide useful constraints (e.g. $V - I = -1.3 \pm 1.0$). We can, however, put limits on the equivalent width from the B- and V-band fluxes, assuming that the B band measures the continuum and the V band the continuum plus line flux, with the same assumptions as used in Paper II. As the equivalent width is directly dependent on the ratio of V-band flux to B-band flux, we estimate an equivalent width lower limit by setting the V-band flux to its $-n\sigma$ excursion and the B-band flux (which is formally measured to be zero) to its positive, $+n\sigma$ value. The resulting rest-frame equivalent width lower limit for $n = 1$ is $\mathrm{EW_r} > 1130$ Å. For $n = 2$, the value is already a rather moderate 57 Å, and the '3σ' result is compatible with both the V and B band just containing pure continuum emission of a flat spectrum source. However, if the observed V-band flux were mostly Lyα emission, $(5.8 \pm 1.2) \times 10^{-17}$ erg cm^{-2} s^{-1} should be easily seen in a spectrum as it is more than two times the flux in the main halo. In this case, the fact that the western edge of the slit is about 3.9 arcsec away from the tail of 4 is likely preventing us from detecting a strong Lyα emission line. It is intriguing that the emission line feature ϵ, though stronger than either δ or γ, which both correspond to galaxies clearly detected, does not have a corresponding broad-band object near enough to the slit to explain the relatively strong signal. Thus, ϵ may just be a small fraction of the line emission from the tail of object 4, spilling over into the slit.

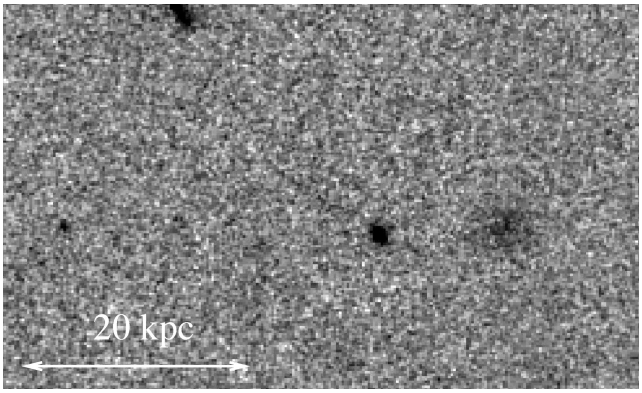

Figure 7. 4.9 arcsec × 7.3 arcsec V-band image of object 4.

3.1 Spatially extended line emission

3.1.1 He II 1640

Aside from the Lyα emission, several other extended emission features can be seen in the spectrum. He II 1640.4 Å is noisy but clearly present near an observed wavelength of 6914 Å. In the spatial direction, it ranges over several arcseconds (Fig. 8). The presence of multiple residuals from the subtraction of sky lines and a strong spatial gradient in the sky background make a flux measurement difficult, but we estimate that the flux is about $(4.5 \pm 1.4) \times 10^{-18}$ erg cm^{-2} s^{-1} (statistical errors only), within a distance of 4.3 arcsec on either side of the continuum trace. Formally, this is approximately 19 per cent of the H I Lyα flux. This comparison with H I should not be taken too serious as He II 1640 is likely to be less optically thick than H I Lyα, so its spatial width may largely reflect the spatial extent of the emitting gas, whereas a substantial fraction of H I Lyα may have been scattered further outside of the slit. Thus, the observed He II 1640/H I Lyα flux ratio may be a considerable overestimate. If we approximate the spatial profile of the Lyα halo

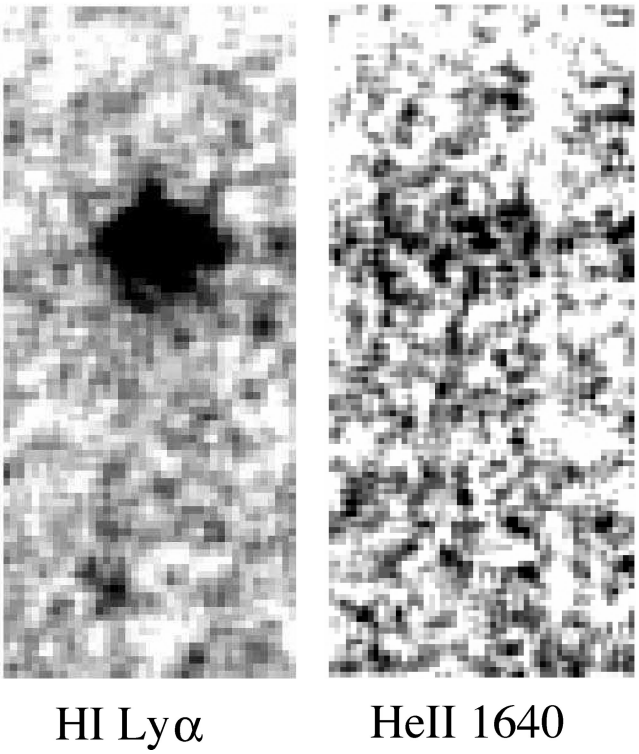

Figure 8. Part of the spectrum showing again the H I Lyα line region, and the corresponding region from the LRIS red arm spectrum, containing He II 1640. The sections have been scaled to have the same velocity (horizontal; width 2960 km s^{-1}) and spatial extent (vertical; 25.6 arcsec). The spatial centre of the sections is somewhat offset to the south of the continuum trace in order to include an apparent spur of emission ending in a bright spot about 13 arcsec to the south. The He II emission is somewhat affected by sky subtraction residuals.

by a circular Gaussian profile with the radius set to the spatial extent *along* the slit (FWHM = 1.9 arcsec), only about 26 per cent of the Lyα emission would have passed through the slit. This could reduce the He II/Lyα to 0.05, a value consistent with several different ionization mechanisms (see the discussions in Yang et al. 2006; Prescott, Dey & Jannuzi 2009; Scarlata et al. 2009).

3.1.2 Metal transitions and extended emission

Several features belonging to metal line transitions can be seen in the one-dimensional spectrum (Fig. 2), including an absorption/emission complex, with the peak emission occurring near 5234.6 Å (FWHM $\sim$ 500 km s^{-1}), possibly related to the N V 1239, 1243 Å doublet, and absorption troughs at 5302.5 and 5418.8 Å. We identify the lower redshift one with the Si II 1260 Å resonance line. A further, broader trough near 5480 Å almost certainly corresponds to the O I/Si II 1302–1304 Å complex often seen in Lyman break galaxies (e.g. Shapley et al. 2003). The low signal-to-noise ratio does not permit a very meaningful analysis, but single-component, Gaussian fits to the absorption troughs at 5302.5 and 5418.8 Å show them to be blueshifted with respect to the nominal redshift from the peak of the Lyα line, $z = 3.2158$, by about -630 and -500 km s^{-1}, with rest-frame equivalent widths of the order of 3 Å.

In several wavelength regions below and above Lyα, the spectral trace seems to be broadened, suggesting spatially extended emission line regions. We show some of these regions in Fig. 9, indicating the spatial correspondence between spectrum and image by dashed lines. To give an idea of the flux levels and significance of the excess emission along the slit, Fig. 10 shows some of the spatial profiles after collapsing the regions in the previous figure along the dispersion direction. Note that an average continuum spectrum has been subtracted in Fig. 10 and the fluxes represent just the excess emission.

Because of the low signal-to-noise ratio, the presence of Lyα forest absorption, and the unknown mechanisms populating the atomic levels, we found it difficult to assign the extended emission to definite transitions. The few identifications suggested here are tentative and may change with better data.

The first region (top panel in Fig. 9) comprises relatively prominent emission extended to both the north and south of tadpole 1. The spectral traces of two other objects, 10 and 7 in Fig. 5, are visible as well just below the trace of the main galaxy for a wavelength stretch of about 50 Å in the rest frame, of which we show the central part in this panel. Having enhanced emission at the same wavelength as the main tadpole would be an argument in favour of these objects sharing the same redshift. Among the transitions in this wavelength range that could produce the band-like spectral character, possible candidates are numerous Fe II and Fe II] lines in the vicinity of 1104 Å, with several transitions from the ground state and accompanying low-lying excited states.

The second panel from the top, shows an asymmetric, extended emission region (1157.3–1161.8 Å) redwards of an absorption trough. The nature of this feature is unclear.

In the third panel of Fig. 9, we find deep absorption troughs just bluewards of extended emission near 1288.7–1294.0 Å and 1302.9–1304.1 Å. The identification of the lower wavelength transition is uncertain, but the spectrally narrow, spatially very extended emission region 1302.9–1304.1 Å most likely corresponds to the O I 1302.17, 1304.86, 1306.02 Å triplet and the Si II 1304.37, 1309.28 Å doublet (with possible contributions by other ions) which would also account for the absorption trough immediately bluewards. Si II may be expected to be the dominant contributor under a wider range of possible physical scenarios, but is perhaps somewhat too far to the red of the optimal position. The spatial extent of the emission appears to exceed that of the other emission regions discussed earlier in both directions along the slit. If the emission is due to O I, it could be enhanced by Bowen fluorescence (Bowen 1947), i.e. pumping of O I by H I Lyβ. A situation like this could arise in the contact zone between partly neutral gas (O I) embedded in more highly ionized gas where recombinations produce Ly series photons.

The fourth panel shows the wavelength region near the expected position of the N V 1239, 1243 Å doublet. N V may be present in the form of an absorption trough, as commonly seen in high-redshift galaxies, plus a faint emission feature (marked as '1241.3 Å'), which is extended to the south. At a flux of $(1.8 \pm 1.2) \times 10^{-18}$ erg cm^{-2} s^{-1}, a comparison with other metals commonly seen in ionized gas, is difficult. The flux at the C IV 1548, 1549 Å doublet position (in a noisy part of the spectrum, and seriously marred by sky residuals; not shown), which is commonly stronger than N V, at $(0.83 \pm 1.5) \times 10^{-18}$ erg cm^{-2} s^{-1} is not significant.

In the bottom panel, a wavelength region from the red side of the spectrum contains a comb-shaped, multiple emission line pattern extending about 2.7 arcsec (21 kpc proper) to the north, unfortunately marred by two background residuals. We tentatively identify the lines between 1658.8–1665.0 and 1666.6–1674.7 Å with O III] 1660, 1666 Å (which most likely would be collisionally excited) and Al II 1671 Å (which could be pumped by continuum radiation).

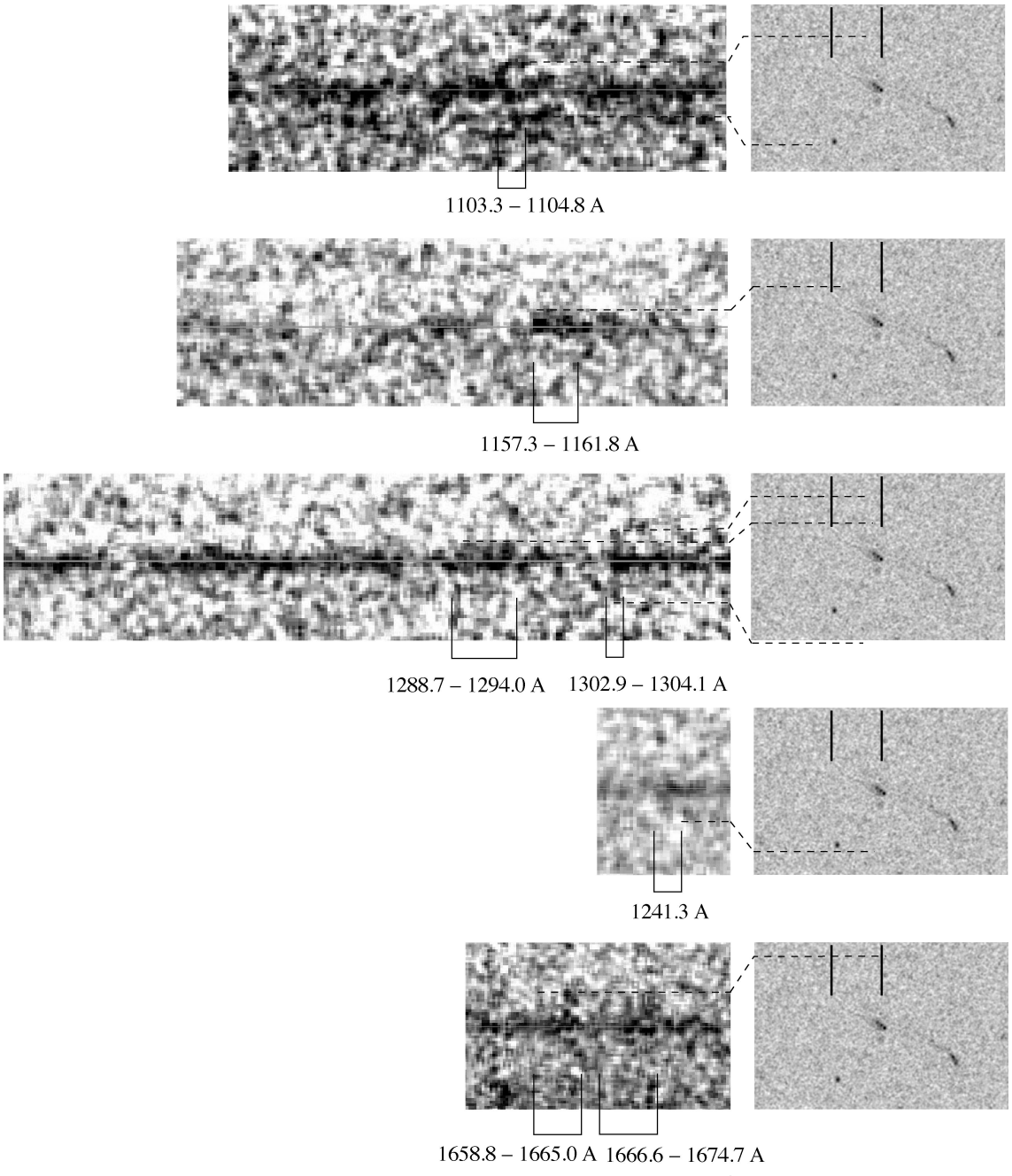

Figure 9. Several individual stretches of the spectrum, showing spatially extended emission features with their rest wavelengths (assuming $z = 3.2158$) and 6.7 arcsec high ACS *F435W* images centred on tadpole 1. The horizontal, thin, light grey solid lines indicate the median position of the continuum in the spatial direction. The black, dashed lines are meant to guide the eye as to the extent of the spectral emission in relation to tadpole 1. The short vertical lines in the ACS image indicate the approximate horizontal position of the slit jaws. The region 1302.9–1304.1 Å is a sharp wavelength feature that extends out on both sides of the continuum, whereas other features are more asymmetric. The significance and lateral extent of some of the regions can be judged from Fig. 10.

4 ORIGIN OF THE LYα EMISSION

The uncertain spatial extent of the Lyα emission beyond the slit prevents a measurement of the escape fraction of Lyα, but we can establish whether there is a source of Lyα sufficiently strong to explain the observed flux. If due to photoionization, the observed flux of Lyα photons requires an ionization rate of about 1.98×10^{53} erg cm^{-2} s^{-1} Hz^{-1}. Under the assumptions made in papers I and II, this can be achieved by a star-forming galaxy with rest-frame luminosity $L_{1500\,\text{Å}} = 2.34 \times 10^{28}$ erg s^{-1} Hz^{-1} or V-band (AB) magnitude = 26.4. With the brightest galaxy, number 1, having a magnitude of 24.9, there nominally are about four times as many ionizing photons available as required to explain the observed Lyα, not counting any of the other sources in the field. Even if the slit losses approached a factor of ∼4, as discussed above, stellar photoionization would remain a viable explanation. Based on the existing data, we cannot rule out the presence of an AGN, but there currently is no evidence for the emission being dominated by such an object.

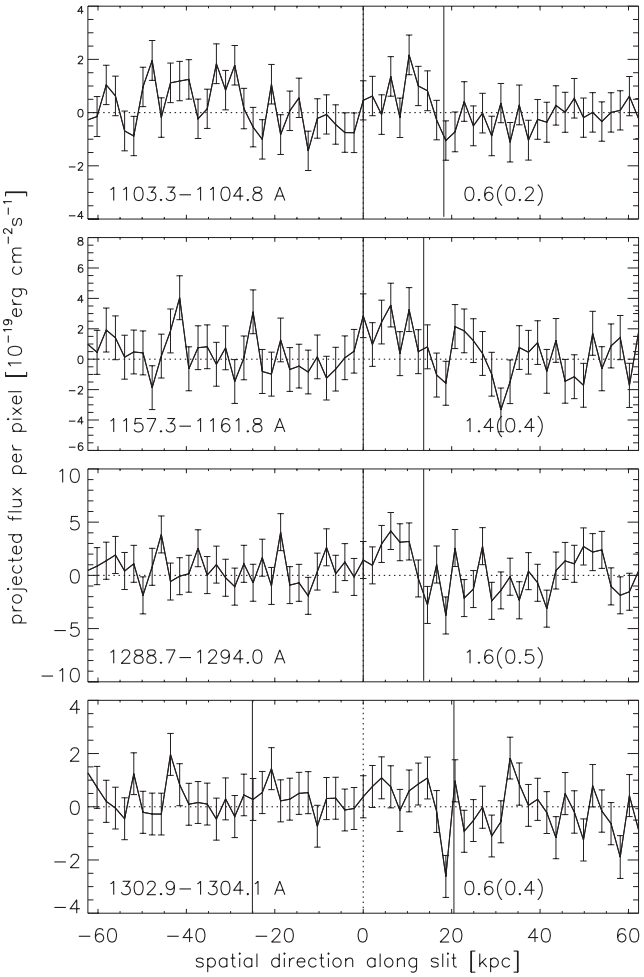

Figure 10. This figure gives an idea of the fluxes, spatial extent, and asymmetry of several of the extended emission line features shown in the previous figure. It shows spatial profiles of the first four spectral segments from Fig. 9, with the origin placed at the median position of the continuum profile. The regions of the spectral features shown in Fig. 9 were collapsed along the dispersion direction, and a mean continuum obtained from a nearby wavelength region was subtracted. The two vertical solid lines in each profile show roughly where the edges of the residual visible emission occur in the 2D spectrum. The total fluxes as measured between the positions along the slit indicated by the vertical lines are the numbers to the right of the wavelength range (together with their 1σ statistical errors in parenthesis) in units of 10^{-19} erg cm^{-2} s^{-1}.

The star formation rate associated with galaxy 1, if estimated by the usual relation (Madau, Pozzetti & Dickinson 1998), is found to be

$$\mathrm{SFR} = 2.9\,\mathrm{M}_\odot\ \mathrm{yr}^{-1} \times \frac{L_{1500}}{2.3 \times 10^{28}\ \mathrm{erg\ s^{-1}\ Hz^{-1}}}. \quad (1)$$

Additional constraints on the nature of the Lyα emission come from the absorption troughs present in the spectrum of galaxy 1, which are all blueshifted by the order of $|v_{\mathrm{abs}}| \sim 500{-}600$ km s^{-1} with respect to the Lyα emission peak. In the case of Lyα emitters associated with Lyman break galaxies, the redshifted velocity of the Lyα emission line with respect to the systemic redshift of the galaxy, is about 2–3 times the absolute value of the (blueshifted) outflow velocity $|v_{\mathrm{abs}}|$. This puts the redshift of the Lyα emission relative to the systemic redshift at between 250 and 600 km s^{-1}, which is well consistent with the range observed for Lyman break galaxies (e.g. Rakic et al. 2011), and would mean that at least the central Lyα peak is highly optically thick. Taken together with the presence of an absorption trough in the 1D spectra (Fig. 2) near 5100 Å, the evidence suggests that the Lyα emission is indeed the red peak of a double-humped profile, with the blue peak strongly suppressed. This conclusion remains somewhat uncertain as we do not know how well the spatial positions of the Lyα emission and the continuum emission overlap. With a dispersion of 240 km s^{-1} arcsec^{-1}, a relative spatial shift between them in the direction across the 2 arcsec wide slit could introduce velocity shifts of up to two times this amount. These uncertainties could be eliminated by future narrow-band imaging of the Lyα emission.

5 INTERPRETATION

As for the nature of the galaxies in the field, most of the objects with a head–tail structure have their heads to the south of the tails (1–5), making it less likely that the features have been produced mainly by tidal (two-body) interactions. Rather, the evidence appears consistent with large-scale ram-pressure stripping (Gunn & Gott 1972; Nulsen 1982) of gas, and recent star formation in the downstream ablated tails.

Ram-pressure stripping has been invoked to explain features seen in several astrophysical environments, including galaxy clusters (e.g. Cayatte et al. 1990; Vollmer & Huchtmeier 2003; Chung et al. 2007; Cortese et al. 2007; Hester et al. 2010; Smith et al. 2010; Yagi et al. 2010; Fumagalli et al. 2011; Arrigoni-Battaia et al. 2012; Fossati et al. 2012), the Milky Way halo (e.g. Lin & Faber 1983), the Local Group (e.g. McConnachie et al. 2007) and in galaxy groups (e.g. Marcolini, Brighenti & D'Ercole 2003; Rasmussen, Ponman & Mulchaey 2006). So far, there is relatively scant observational evidence for this process at high redshift, with the exception of the tadpole galaxies, a population of galaxies increasingly common with redshift (e.g. Straughn et al. 2006), that may partly have been shaped by ram-pressure (Elmegreen & Elmegreen 2010).

A particular interesting consequence of ram-stripping is the formation of stars in the stripped gas, which has been the subject of recent observational (e.g. Hester et al. 2010; Smith et al. 2010; Fumagalli et al. 2011; Boissier et al. 2012; Owers et al. 2012; Yoshida et al. 2012) and theoretical study (e.g. Kapferer et al. 2009; Tonnesen & Bryan 2012, see also the Lyα emitting filament in Paper II, which may have a similar origin). Several strands of evidence suggest that the current situation is indeed an instance of star formation in galactic wakes: the tails of most of the objects have blue colours, indicative of very young stars. The finding of extended metal line emission outside of the galaxies is consistent with the presence of a stripped, or re-created, interstellar medium (ISM) that is being excited by the newly forming stars. The high Lyα equivalent width suggested by the tail of galaxy 4 may be another sign of hot, young stars, as discussed in Paper II.

Groups of galaxies falling into clusters seem to produce Hα morphologies similar to the galaxy contrails observed here (e.g. Cortese et al. 2006; Owen et al. 2006; Sun, Donahue & Voit 2007; Yoshida et al. 2012). In the present case, a number of observational details closely resemble hydrodynamic features predicted from simulations of supersonic motions in galaxy clusters (e.g. Roediger, Brüggen & Hoeft 2006; Zavala et al. 2012): the main tadpole 1 shows a shape reminiscent of a bow shock, with a projected tangential angle of close to 45 deg (indicating, at face value, motion with a moderate Mach number ∼1.5), and what looks like a turbulent wake consisting of a vortex street with a longitudinal extent of about 12 kpc and a maximum width of about 5 kpc (Fig. 11). A faint, linear structure

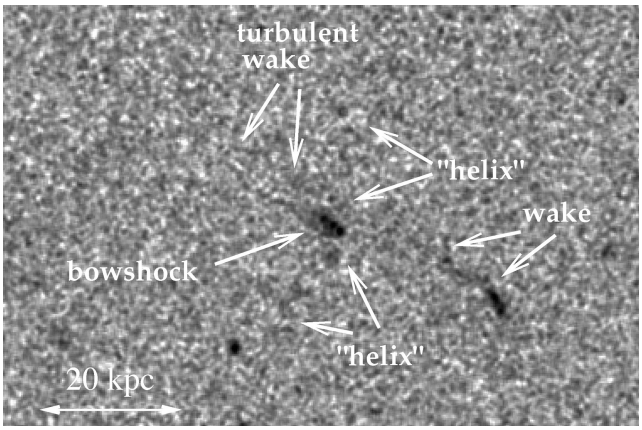

Figure 11. Gas dynamical features indicative of interactions between the galaxies 1 and 2 and the IGM. The height of the image is 7.5 arcsec.

vaguely resembling a 'helix' extends almost perpendicular to the axis of symmetry (i.e. the head–tail direction) to both sides of the galaxy, with a maximum traceable extent of ∼20 kpc to the south and somewhat less to the north. The nature of this feature is not clear. Some of the extended emission seen in Fig. 9 appears to arise from that region, suggesting that it may be associated with both low and highly ionized gas. The pattern with the 'helical' appearance could perhaps arise through hydrodynamic instabilities. A broadening tail of vortices (e.g. Roediger et al. 2006, their fig. 4), may look similar, if the tadpole were viewed almost frontally, moving towards the observer, and the 'helical' structure were on the far side of the tadpole. Similar curly structures also occur in the wakes of *interacting* galaxies undergoing stripping (e.g. Kapferer et al. 2008, their fig. 9). Alternatively, the apparent spiral pattern may suggest a passing, rotating small galaxy with an asymmetric outflow of gas that traces out a helical pattern. If the structure were an outflow from the tadpole galaxy 1, e.g. the helical jet of an AGN, a large outflow velocity faster than the relative velocity between galaxy and ambient gas could explain why the 'helices' are not being swept back at a sharper angle.

5.1 Morphological and colour changes as a consequence of ram-pressure stripping?

The interpretation of the galaxies being transformed by ram-pressure stripping is largely independent of the question whether all these objects are at the same redshift. Without better spectroscopic redshifts we cannot rule out a situation where the main object 1 is the only one at redshift $z = 3.21$, and the other blue objects and the various tails of emission are chance coincidences in projection of galaxies at lower redshift, as suggested, e.g. by the low photometric redshifts for objects 2 and 4 (0.825 and 0.900; Conselice et al. 2011), and perhaps by the detection of significant U-band light for object 2, and, in one case (object 10), the spectroscopic detection of flux below the high-redshift Lyman limit. In this case, the galaxies – except for object 1 – would not have anything to do with the Lyα halo. For the sake of exploring its physical consequences, however, we will, in the following, uphold the hypothesis of all objects being at the same redshift.

It is tempting to speculate about the origin of the differences in morphological appearance and colour among the three main tadpole galaxies, 1, 2, and 4 along their apparently common direction of motion as reflections of a changing astrophysical environment. Unlike tadpole 1, the object 2 does not show a discernible bow shock, and has a narrower wake. The object 4 that we associated tentatively with high equivalent width Lyα emission exhibits a linear, thin tail (Figs 6 and 7), reminiscent of the expected outcome of Bondi–Hoyle accretion (Sakelliou 2000). The spatial sequence from tadpole 4 to 2 to 1 (Fig. 6) could be interpreted as indicating passage through a zone with a significant temperature gradient (perhaps an accretion shock) from a colder to a hotter gaseous medium: the tadpole 4, which is most advanced in the direction of the flow, with its linear, apparently non-turbulent tail, may be experiencing the higher viscosity and thermal pressure of a hotter environment (e.g. Roediger & Brüggen 2008). Tadpole 2 looks more turbulent, but the tail is still narrow, and it does not have a bow shock either. Tadpole 1 would exhibit a bow shock, if it were on the colder side of the interface between hot and cold gas, and its velocity relative to the IGM exceeded the sound speed for the colder gas. This condition would easily be satisfied when passing through the general filamentary IGM with even moderate velocity, as the typical temperature at $z \sim 3$ is only a few times 10^4 K (Rauch et al. 1996), corresponding to sound speeds of a few tens of km s^{-1}. The tail of tadpole 1 is flaring up and shows a turbulent vortex pattern, consistent with the lower viscosity expected in a colder medium.

We note that the galaxies most advanced into the flow, 2 and 4, both with $B - V \sim 0.1$, have bluer colours, much bluer than the apparently lagging object 1 ($B - V = 1.1$). If we apply a colour correction of $\delta = -0.4$ to account for the $z = 3.2$ Lyα forest absorption (see above), these colours become $B - V = -0.3$ and 0.7, respectively. For the two blue objects 2 and 4, this corresponds to an extreme continuum slope of ~ -3, which is not commonly encountered in high-redshift galaxies. However, these galaxies may be very different from those usually studied at high redshift, which are most often selected by the existence of a Lyman break (e.g. Shapley et al. 2003). It has been argued that the suppression of nebular emission is capable of making the spectrum of a metal-poor starburst galaxy much bluer (e.g. Raiter et al. 2010). Stripping gas off stellar populations would naturally reduce or suppress the nebular emission and reduce the opacity at the Lyman limit, turning the continuum in the stripped galaxy bluer. Even the broad-band colours of the stars forming in the stripped wake may be bluer as they are likely to form in a lower column density environment, be young, and possibly form from the metal-poor gas of the surrounding IGM. If this picture is correct, the two blue objects 2 and 4 may have undergone substantial stripping already, whereas the redder object 1 further out, with its ISM partly protected from stripping by an apparent bow shock, may still have retained more of its nebular emission.

5.2 The astrophysical environment of stripped galaxies at high redshift

The usual condition for ram-pressure stripping to take place is that the ram-pressure on the gas in a galaxy, experienced when passing through the IGM, needs to exceed the gravitational binding force per surface area, $\rho v^2 \geq (\pi/2) G M(< R) \rho_{\rm gal}(R)/R$ (e.g. McCarthy et al. 2008). Here, ρ is the ambient gas density, v the relative velocity of galactic gas and ambient IGM, and G, R, $M(< R)$, and $\rho_{\rm gas}$ are the gravitational constant, the distance of a given gas volume element from the centre of the galaxy, the total gravitating mass internal to that radius, and the galactic gas density, respectively. It has often been assumed that ram-pressure stripping is most relevant for low-redshift, massive clusters. However, the hierarchical nature of structure formation, leading to more compact gravitational potential wells, higher gas densities, and higher interaction rates at

$z \sim 3$ (when compared to the local Universe) suggests that one should expect miniature versions of the ram-pressure stripping seen in low-redshift clusters to occur among satellites in individual high-z galactic haloes. With the higher density at high redshift favouring a higher pressure for a given velocity, the infalling satellites themselves collapse from a denser background as well; so for the effect of ram-pressure stripping, one would have to look mostly to lower mass, dwarf galaxies, perhaps aided by processes that may lower the binding energy of the gas further. The higher merger rate at high redshift may also work to increase the amount of ram-pressure-stripped gas (e.g. Domainko et al. 2006; Kapferer et al. 2008), as may stellar or galactic outflows, as long as they can offset a significant part of the gravitational binding energy. In addition, new cosmological hydrosimulation techniques suggest more efficient stripping (e.g. Hess & Springel 2012) and the presence of puffed up, high-angular momentum gas (e.g. Keres et al. 2012), 'ready to go'.

Recently, it has been argued (Benitez-Llambay et al. 2013) that, in particular, dwarf galaxies do not even require the encounter with fully formed massive haloes but can lose gas to ram-pressure stripping in large-scale structure filaments at high redshift when entering terminal nodes like the (future) Local Group pancake. In this case, our spectrograph slit may have intersected a filament of the cosmic web, lit up by the star formation in the ablated contrails of a swarm of coherently moving galaxies. To attain the high relative velocities required for stripping, the galaxies would have to move highly supersonically with respect to the gas they are plunging into. While we appear to be seeing one galaxy with a bow shock, it is not clear if the velocities of the other objects are high enough for this to work. However, as argued above, the presence of an accretion shock in the terminal node with hot gas on one side may make this scenario consistent with the observations. A variant of this picture may explain the stripping and the apparent gradient in the properties of the tadpoles as a group of galaxies being 'hosed down' when obliquely passing an accreting stream of gas.

5.3 Metal enrichment and escape of ionizing radiation from star formation in stripped gas

The existence of such extended structures at high redshift, the relatively large number density of galaxies with tidal or ram-pressure-related features (see also the disturbed haloes described in papers I and II), and the presence of multiple sites of star-formation in a common gaseous halo or large-scale filament suggest that the stripping of gas from galaxies in interactions could be an important contributor to the metal enrichment of the IGM, analogous to the lower redshift process leading to the enrichment of the gas in galaxy clusters. To explain the finding of metal enrichment in the IGM at large distances from the nearest bright galaxy, galactic winds from Lyman break galaxies have been invoked to drive metal-enriched gas far into intergalactic space (e.g. Pettini et al. 2001; Steidel et al. 2010). Among the persistent uncertainties with this scenario is that the actually observed ranges of galactic winds invariably fall short of accounting for the metals seen in QSO absorption systems at large distances from such galaxies. However, if, as we have argued above, ram-pressure stripping of infalling galaxies and star formation in the stripped wake operate at high redshift, there may be less need to invoke long-range winds from the central galaxy of a halo. In this alternative picture, the ram-pressure that led to the ablation of gas and subsequent star formation may also act to dispel newly formed metal enriched gas from the tails, aided by stellar winds and supernova explosions that would find it much easier to escape from the more weakly bound star-forming regions of galactic wakes. In any case, differential motion between the lost gas and the parent star-forming galaxies will distribute the gas spatially over time. The assumption that this process mostly occurs in infalling objects implies that the gas is automatically reaching distances from any brightest halo galaxy as large as commonly observed (in metal absorption lines; e.g. Chen 2012). Tidal interactions may lead to a similar result: metals are expelled into the gaseous halo of brighter galaxies that came from the shredded ISM of its satellites or from outflows in tidal tails or dwarfs, and both processes may exist among the extended, asymmetric Lyα emitters in our study. There may be differences between the metallicities of the gas ejected from tidal star-forming regions, and the gas lost by star-forming regions in galactic contrails. Stars in the former arise from the relatively metal-rich ISM of the parent galaxy, as would stars in gas ablated by ram-pressure or viscous stripping. Stars forming in turbulent wakes behind the galaxies may feed on the lower metallicity gas in the halo or IGM as well, which may contribute to the signatures of hot, young stars described in Paper II.

We have argued earlier in Paper II that extragalactic star formation in the wakes of stripped galaxies and in tidal tails may facilitate the production and escape of ionizing photons and may have brought about the reionization of the Universe at high redshift. Stripping gas off stellar populations may not only explain the very blue continuum slopes of some of the galaxies in the present case through suppression of nebular emission, but would also simultaneously lead to lines of sight with reduced optical depth for ionizing photons. Blue colours of 'naked' stellar populations may be the smoking gun of escaping ionizing radiation. Even in the stripped wakes, the presence of young, massive stars, and the weak gravitational binding force enabling easy removal of neutral gas by even moderate amounts of stellar winds or supernova outflows, would all tend to enhance the escape of ionizing radiation. Recently, Bergvall et al. (2013), examining selection effects in the search for local galaxies leaking ionizing radiation, have come to similar conclusions as to the likely conditions required, including the importance of stripping.

6 CONCLUSIONS

We have detected an emission line halo that we identify as Lyα emission at $z = 3.21$, with several faint filaments stretching over tens of kpc. Spatially, the filaments overlap in projection with star-forming regions in the form of mostly blue, faint galaxies, several of which have a distinct tadpole shape and blue, partly turbulent tails, with one object showing what appears to be a bow shock. The GOODS-N ACS *F*435*W* image reveals several such features criss-crossing an area several times bigger than the visible extent of the Lyα halo. The emission of the central halo and of the filaments is broadly consistent with being powered by stellar photoionization. We detect spatially extended emission lines from gas surrounding the main tadpole, including He II 1640, and possibly N V 1240, O III], Al II, and Fe II, suggesting an extended, extragalactic, ISM with current star formation.

The current observations allow for the possibility that the faint blue galaxies are lower redshift, foreground objects that are seen in chance projection against the Lyα halo of the main, $z = 3.21$, galaxy, GOODS J123646.84+621608.1 (our object 1).

The tadpole shapes, partial alignment, and the considerable numbers of unusual broad-band objects make it unlikely that the features observed are pre-dominantly tidal in origin (i.e. caused by individual two-body encounters). Instead, the galaxies may have experienced stripping of gas when moving relative to the intergalactic or intrahalo medium, with stars forming downstream in the

galactic contrails. This process is observationally and theoretically well established in the local Universe. Our observations may have identified an occurrence of ram-pressure stripping at high redshift, possibly involving satellite galaxies interacting with the gas in more massive, individual galactic haloes. The filamentary structure trailing behind a galaxy in the $z = 2.63$ halo described in Paper II may be another example of this effect. In the present case, the morphologies and colours of several tadpoles change along their general direction of motion, which may be consistent with these galaxies passing into a hotter gaseous environment, possibly the region behind an accretion shock. Such a stripping scenario may play out on a larger scale when differential motions of galaxies relative to the nodes in the gaseous cosmic web strip galaxies off their gas, as suggested by Benitez-Llambay et al. (2013). As in the case of local clusters, the galactic contrails should be able to release metal-enriched gas, perhaps enhanced by local stellar feedback, more easily than normal galaxies. At the very least, these objects should provide a contribution to the intergalactic metal budget of galactic haloes. The loss of enriched gas from galactic contrails may suggest a solution to the long-standing puzzle of how the IGM at large distances from bright galaxies was polluted with metals.

Stripping of gas from existing stellar populations would not only create pathways for the escape of ionizing radiation, but may also explain the very blue continuum colours of some objects through the suppression of nebular emission. Star formation in galactic contrails may produce young, hot stars, surrounded by lower than typical H I gas column densities, and capable of clearing their environment of gas, altogether suggesting a way in which galaxies can ionize the IGM.

ACKNOWLEDGEMENTS

The data were obtained as part of a long term collaboration with the late Wal Sargent, to whose memory we dedicate this paper. We thank the anonymous referee for useful and critical suggestions that led to clarifications and improvements of the paper. We acknowledge helpful discussions with Guillermo Blanc, Bob Carswell, Michele Fumagalli, and Andy McWilliam. We thank the staff of the Keck Observatory for their help with the observations. MR is grateful to the National Science Foundation for grant AST-1108815. GB has been supported by the Kavli Foundation, and MGH received support by the European Research Council under the European Union's Seventh Framework Programme (FP/2007-2013) / ERC Grant Agreement no. 320596. JRG acknowledges a Millikan Fellowship at Caltech. We acknowledge use of the Atomic Line List v2.05, maintained by Peter van Hoof and the use of the NIST Atomic Spectra Database (ver. 5.0; Kramida et al. 2012). This research has further made use of the NASA/IPAC Extragalactic Database (NED) which is operated by the Jet Propulsion Laboratory, California Institute of Technology, under contract with the National Aeronautics and Space Administration, and of the VizieR catalogue access tool.

REFERENCES

Arrigoni-Battaia F. et al., 2012, A&A, 543, 112
Benitez-Llambay A., Navarro J. F., Abadi M. G., Gottlöber S., Yepes G., Hoffman Y., Steinmetz M., 2013, ApJ, 763, 41
Bergvall N., Leitet E., Zackrisson E., Marquart T., 2013, A&A, 554, A38
Boissier S. et al., 2012, A&A, 545, 142
Bowen I. S., 1947, PASP, 59, 196
Capak P. et al., 2004, AJ, 127, 180
Cayatte V., van Gorkom J. H., Balkowski C., Kotanyi C., 1990, AJ, 100, 604
Chen H.-W., 2012, MNRAS, 427, 1238
Chung A., van Gorkom J. H., Kenney J. D. P., Vollmer B., 2007, ApJ, 659, 115
Conselice C. J. et al., 2011, MNRAS, 413, 80
Cooke J., Berrier J. C., Barton E. J., Bullock J. S., Wolfe A. M., 2010, MNRAS, 403, 1020
Cooke J., Omori Y., Ryan-Weber E., 2013, MNRAS, 433, 2122
Cortese L., Gavazzi G., Boselli A., Franzetti P., Kennicutt R. C., O'Neil K., Sakai S., 2006, A&A, 453, 847
Cortese L. et al., 2007, MNRAS, 376, 157
Domainko W. et al., 2006, A&A, 452, 795
Elmegreen B. G., Elmegreen D. M., 2010, ApJ, 722, 1895
Fossati M., Gavazzi G., Boselli A., Fumagalli M., 2012, A&A, 544, 128
Fumagalli M., Gavazzi G., Scaramella R., Franzetti P., 2011, A&A, 528, 46
Giavalisco M. (GOODS Team), 2004, ApJ, 600, L93
Gunn J. E., Gott J. R., III, 1972, ApJ, 176, 1
Hamana T., Ouchi M., Shimasaku K., Kayo I., Suto Y., 2004, MNRAS, 347, 813
Hayashino T. et al., 2004, AJ, 128, 2073
Hess S., Springel V., 2012, MNRAS, 426, 3112
Hester J. A. et al., 2010, ApJ, 716, 14
Inoue A. K., 2010, MNRAS, 401, 1325
Kapferer W., Kronberger T., Ferrari C., Riser T., Schindler S., 2008, MNRAS, 389, 1405
Kapferer W., Sluka C., Schindler S., Ferrari C., Ziegler B., 2009, A&A, 499, 87
Keres D., Vogelsberger M. Sijacki D., Springel V., Hernquist L., 2012, MNRAS, 425, 2027
Kovac K., Somerville R. S., Rhoads J. E., Malhotra S., Wang J. X., 2007, ApJ, 668, 15
Kramida A., Ralchenko Yu., Reader J., and the NIST ASD Team, 2012, National Institute of Standards and Technology, Gaithersburg, MD
Lin D. N. C., Faber S. M., 1983, ApJ, 266, 21
McCarthy J. K. et al., 1998, Proc. SPIE, 3355, 81
McCarthy I. G., Frenk C. S., Font A. S., Lacey C. G., Bower R. G., Mitchell N. L., Balogh M. L., Theuns T., 2008, MNRAS, 383, 593
McConnachie A. W., Venn K. A., Irwin M. J., Young L. M., Geehan J. J., 2007, ApJ, 671, 33
Madau P., Pozzetti L., Dickinson M., 1998, ApJ, 498, 106
Marcolini A., Brighenti F., D'Ercole A., 2003, MNRAS, 345, 1329
Matsuda Y. et al., 2012, MNRAS, 425, 878
Meiksin A., 2006, MNRAS, 365, 807
Nulsen P. E. J., 1982, MNRAS, 198, 1007
Oke J. B., Cohen J. G., Carr M., Cromer J., Dingizian A., Harris F. H., 1995, PASP, 107, 375O
Ouchi M. et al., 2009, ApJ, 696, 1164
Owen F. N., Keel W. C., Wang Q. D., Ledlow M. J., Morrison G. E., 2006, AJ, 131, 1974
Owers M. S., Couch W. J., Nulsen P. E. J., Randall S. W., 2012, ApJ, 750, L23
Pellerin A., Robert C., 2007, MNRAS, 381, 228
Pettini M., Shapley A. E., Steidel C. C., Cuby J.-G., Dickinson M., Moorwood A. F. M., Adelberger K. L., Giavalisco M., 2001, ApJ, 554, 98
Prescott M. K. M., Dey A., Jannuzi B. T., 2009, ApJ, 702, 554
Prochaska J. X., Worseck G., O'Meara J. M., 2009, ApJ, 705, 113
Raiter A., Schaerer D., Fosbury R. A. E., 2010, A&A, 523, 64
Rakic O., Schaye J., Steidel C. C., Rudie G. C., 2011, MNRAS, 414, 3265
Rasmussen J., Ponman T. J., Mulchaey J. S., 2006, MNRAS, 370, 453
Rauch M., Sargent W. L. W., Womble D. S., Barlow T. A., 1996, ApJ, 467, 5
Rauch M. et al., 2008, ApJ, 681, 856
Rauch M., Becker G. D., Haehnelt M. G., Gauthier J.-R., Ravindranath S., Sargent W. L. W., 2011, MNRAS, 418, 1115 (Paper I)
Rauch M., Becker G. D., Haehnelt M. G., Gauthier J.-R., Sargent W. L. W., 2013a, MNRAS, 429, 429 (Paper II)
Rauch M., Becker G. D., Haehnelt M. G., Carswell R. F., Gauthier J.-R., 2013b, MNRAS, 431, 68 (Paper III)
Roediger E., Brüggen M., 2008, MNRAS, 388, 89

Roediger E., Brüggen M., Hoeft M., 2006, MNRAS, 371, 609
Sakelliou I., 2000, MNRAS, 318, 1164
Scarlata C. et al., 2009, ApJ, 706, 1241
Schaerer D., 2003, A&A, 397, 527
Shapley A. E., Steidel C. C., Pettini M., Adelberger K. L., 2003, ApJ, 588, 65
Smith R. J. et al., 2010, MNRAS, 408, 1417
Steidel C. C., Shapley A. E., Pettini M., Adelberger K. L., Erb D. K., Reddy N. A., Hunt M. P., 2004, ApJ, 604, 534
Steidel C. C., Erb D. K., Shapley A. E., Pettini M., Reddy N., Bogosavljevic M., Rudie G. C., Rakic O., 2010, ApJ, 717, 289
Straughn A. N., Cohen S. H., Ryan R. E., Hathi N. P., Windhorst R. A., Jansen R. A., 2006, ApJ, 639, 724
Sun M., Donahue M., Voit G. M., 2007, ApJ, 671, 190
Tonnesen S., Bryan G. L., 2012, MNRAS, 422, 1609
Vollmer B., Huchtmeier W., 2003, A&A, 406, 427
Xue Y. Q. et al., 2011, ApJS, 195, 10
Yagi M. et al., 2010, AJ, 140, 1814
Yang Y., Zabludoff A. I., Davé R., Eisenstein D. J., Pinto P. A., Katz N., Weinberg D. H., Barton E. J., 2006, ApJ, 640, 539
Yoshida M., Yagi M., Komiyama Y., Furusawa H., Kashikawa N., Hattori T., Okamura S., 2012, ApJ, 749, 43
Zavala J., Balogh M. L., Afshordi N., Ro S., 2012, MNRAS, 426, 3464
Zheng Z., Cen R., Trac H., Miralda-Escudé J., 2011, ApJ, 726, 38

This paper has been typeset from a TEX/LATEX file prepared by the author.